AIAA JOURNAL
Vol. 42, No. 9, September 2004

Using Heterogeneous Propellant Burning Simulations as Subgrid Components of Rocket Simulations

L. Massa,* T. L. Jackson,† and J. Buckmaster‡
University of Illinois at Urbana–Champaign, Urbana, Illinois 61801

We discuss the manner in which one-dimensional unsteady descriptions can be constructed from multidimensional unsteady simulations of heterogeneous propellant combustion. Spatial averaging of the heat equation within the propellant is used to generate a one-dimensional equation with a number of source terms defined by the multidimensional thermal field and surface corrugations. Each of these terms is evaluated numerically, and those that can be neglected are identified; models are defined and tested for those that cannot. Closure of the one-dimensional description is achieved by relating the mean surface regression rate and the heat flux from the combustion field at the surface to the pressure and the average surface temperature. These relations are in the form of a look-up table generated from the "exact" (multidimensional) simulations. The accuracy of the one-dimensional system is tested by comparing the predictions with those of the exact model. This is done for steady burning rates at various pressures and for the unsteady burning response to pressure ramps and pressure pulses.

Nomenclature

c	=	specific heat
f	=	surface function
g	=	$\bar{T}_\eta$ at the surface
L	=	half-width of propellant pack element
M	=	mass flux
n	=	distance measured along normal to surface
P	=	spatially uniform background pressure
R	=	universal gas constant
r_b	=	surface regression rate
S	=	source terms in heat equation
T	=	temperature
t	=	time
t_h	=	midpoint of the pressure pulse, pressure ramp
x	=	distance measured nominally parallel to the surface
y	=	distance measured nominally perpendicular to the surface
α_v	=	volume fraction of ammonium perchlorate
δ	=	timescale of the pressure pulse and pressure ramp
η	=	mapping defined by Eq. (7)
λ	=	heat conductivity
ρ	=	density

Subscripts

AP	=	ammonium perchlorate
binder	=	binder
c	=	condensed phase
homog.	=	determined by homogenization theory
s	=	surface

Superscripts

ˆ	=	surface average
¯	=	spatial average (x-wise)

Received 7 August 2003; revision received 2 April 2004; accepted for publication 19 April 2004.

*Postdoctoral Associate, Center for Simulation of Advanced Rockets, 1304 W. Springfield Avenue; lucal@csar.uiuc.edu.

†Senior Research Scientist, Center for Simulation of Advanced Rockets, 1304 W. Springfield Avenue; tlj@csar.uiuc.edu.

‡Professor, Department of Aerospace Engineering, 104 S. Wright Street; limey@uiuc.edu.

I. Introduction

WE are concerned with the contribution that numerical simulations of heterogeneous propellant combustion can make to the numerical simulation of the chamber flows in large-scale solid-propellant rockets. This is a challenging problem because the numerical grid for the chamber flow might be measured on the centimeter scale,[1] whereas that for the combustion simulations is on the 1–10 μm scale.[2] Moreover, the largest length scale relevant to the combustion problem is defined by the largest particles in the propellant and is usually much less than 1 mm. In short, the combustion simulations are subgrid ingredients of the chamber simulations, and evaluation of their macroscopic contribution is nontrivial.

On the chamber-flow scale the combustion field is a sheet in which gas flow from the solid surface is heated three- or fourfold (in degrees Kelvin). Some of the heat generated within this sheet is conducted toward the surface and plays the dominant role in defining the magnitude of the gas flow. There is a thermal layer in the solid itself, which is also a sheet, one in which transient storage of energy can occur, which also affects the gas flow.

An important difference between the combustion zone in the gas and the thermal layer in the solid is defined by their natural timescales. Because of the density difference, the solid timescale is much greater than the gas timescale, and there are circumstances when it is appropriate to advance the chamber flow on the long scale in a fully coupled fashion.[3] Then the equations of turbulent flow are integrated in the chamber at the same time that a quasi-one-dimensional heat equation is integrated in the solid, with appropriate coupling at the chamber walls.

In past work, the solid-phase heat-conduction equation and its ingredients are, necessarily, presented as a starting point, not something to be derived from the underlying multidimensional description. Absent that multidimensional description, what other choice is there? Thus, one possible formulation, one that subsumes any near-surface heterogeneous reaction layer into a surface discontinuity, goes as follows:

In a frame attached to the nominally plane surface, which recedes uniformly but unsteadily and defines a mass flux $M(t) = \rho_c r_b$, heat conduction is governed by the equation

$$c_c\left(\rho_c \frac{\partial T}{\partial t} + M\frac{\partial T}{\partial n}\right) = \lambda_c \frac{\partial^2 T}{\partial n^2} \tag{1}$$

when n is measured normal to the surface. Here, ρ_c and λ_c are averages of variables that differ significantly among the propellant components.

Deep within the surface (on the scale λ_c/Mc_c) the temperature is uniform and

$$T \to T_o \qquad \text{as} \qquad n \to -\infty \tag{2}$$

At the surface ($n=0$) things are a little more complicated, but let us suppose, for the moment, that the problem is genuinely one-dimensional, as it would be for a homogeneous propellant. The composition of the propellant is specified, so that if M were known the reactant fluxes at $n=0^+$ would be known. These fluxes, the surface temperature, and the pressure are sufficient to determine the combustion field, in principle, and therefore they determine the conductive heat flux to the surface $n=0^+$, from which can be calculated the heat flux at the surface within the solid ($n=0^-$) once the energetic consequences of the surface discontinuity are accounted for. Thus we can write

$$\frac{\partial T}{\partial n}(n=0^-) = g \tag{3}$$

where g is a function of M, T_s (the surface temperature), and P (the pressure).

The formulation is complete if a prescription for the determination of M is given, and a common choice is the simple pyrolysis law

$$M = A_s \exp(-B_s/RT_s) \tag{4}$$

Equation (3) is then a nonlinear mixed boundary condition, one that relates the surface temperature and the surface heat flux.

We now assume, for the heterogeneous propellant, that the formulation (1–4) is still appropriate where g now accounts, in some average fashion, for the multidimensional combustion field, and the pyrolysis law (4) properly represents an average of the regression of the individual components of the propellant.

The shortcomings of this strategy are clearly evident. The field equation (1) in no way reflects the surface irregularities, irregularities that occur on a small length scale but whose average contribution is not necessarily negligible on that account. Appropriate choices for the averages ρ_c and λ_c are not self-evident. The functional nature of g is left unspecified, and it is difficult to think of a sensible strategy for modeling this function absent a detailed description of the combustion field. And how one should specify the pyrolysis law (4) in a way that is consistent with the individual regression laws is also left undefined.

And so we now define the fundamental goal of the present paper. It is to discuss in detail the issues that arise when an attempt is made to derive a one-dimensional description such as expressions (1–4) from an underlying multidimensional description and to provide a description of one such model, albeit imperfect. An essential tool that makes this possible, and that was unavailable to previous workers, is a suite of codes and theory that permit the numerical description of heterogeneous propellant combustion. The house name for this suite within the Center for Simulation of Advanced Rockets at the University of Illinois is Rocfire.[§] The house name for the one-dimensional description is Rocburn. And so we can phrase our quest thus: how do we construct Rocburn from Rocfire in a rational fashion?

The structure of the paper is as follows:

1) We first discuss heat conduction within the propellant in a frame attached to the surface and average over x to generate a one-dimensional heat equation with source terms (S), averages of small-scale two-dimensional fluctuations. A simple model shows it unlikely that all of the source terms are negligible.

2) Certain terms in the averaged description, apart from S, can only be specified using the two-dimensional simulations, and this is handled by constructing a look-up table. The table inputs are the mean surface temperature and the pressure, and the outputs include the mean surface regression rate and the mean surface heat flux. A simple strategy for constructing the table is to vary the surface temperature by varying the cold supply temperature (T_o), and this strategy is described in detail.

3) We examine the various terms in S and use two-dimensional simulations to evaluate their contribution to the mean surface temperature because that, along with the pressure, controls the mean burning rate. The simulations examine the response of the propellant to a pressure pulse. In this way those terms in S that can be neglected are identified. Some cannot be neglected and are modeled, albeit crudely. The models are tested by examining varations in the mean surface temperature during a pressure pulse.

4) The various terms in S affect the global heat balance within the propellant, and this balance can be properly captured, even if S is set equal to zero, by adjusting the heat-flux boundary condition at the propellant surface. In this way the difficulties with the modeling of S are bypassed, and so we discuss this strategy.

5) An alternative strategy to that described in item 3 is used to construct the look-up table. This uses oversampling of the two-dimensional output during a complicated pressure history, with a least-squares approximation for the table entries.

6) Finally, because the whole purpose of our analysis is to construct a one-dimensional model that can be used as a substitute for the two-dimensional calculations in an integrated (macroscopic scale) code, we compare the one-dimensional response to a pressure pulse with the exact calculations for three cases: $S=0$ with the modified boundary condition, T_o controlled look-up table; S modeled, T_o controlled look-up table; S modeled, look-up table constructed by sampling.

II. Heat Conduction Within the Solid

The equation to be solved in the thermal layer (of nominal thickness λ_c/Mc_c) is (with the subscripts dropped)

$$\rho c \frac{\partial T}{\partial t} = \nabla \cdot (\lambda \nabla T) \tag{5}$$

where it is assumed that the specific heat c is a constant and ρ and λ are each piecewise constants with two values, one in the oxidizer and the other in the fuel binder. The propellant is assumed to be a mix of ammonium perchlorate (AP) and hydroxyl-terminated-polybutadiene, but the strategies that are discussed have general applicability. Because the discussion requires the results of a significant number of Rocfire simulations, we shall only examine the two-dimensional problem, as our immediate goal is to identify the difficulties and explore strategies for overcoming them. We expect this to significantly simplify the eventual generation of a Rocburn module rooted in three-dimensional simulations.

Assume that the location of the propellant surface is defined by

$$y = f(x,t) \tag{6}$$

where f is a singe-valued function, y is measured in a direction that is nominally normal to the surface, and x is measured in a direction that is nominally parallel to the surface. This description cannot accommodate cracks, or the detachment of solid particles from the surface, but is an ingredient of most of our Rocfire simulations. A level-set strategy that is not subject to these limitations is described in Ref. 4, but it is not clear that this could provide a framework from which a Rocburn module could be created.

Equation (5) is now written in a frame tied to the propellant surface by using the coordinate transformation

$$x, y, t \to x, \eta = y - f(x,t), t \tag{7}$$

whence

$$\rho c(T_t - f_t T_\eta) = (\lambda T_x)_x + \left(1 + f_x^2\right)(\lambda T_\eta)_\eta - f_{xx}\lambda T_\eta - f_x[(\lambda T_\eta)_x + (\lambda T_x)_\eta] \tag{8}$$

There is an obvious connection with Eq. (1) with η playing the role of n and $-\rho f_t$ corresponding to the mass flux M, but a quasi-one-dimensional description must arise from averaging Eq. (8) over x,

[§]Information available online at http://www.csar.uiuc.edu/~tlj/rocfire.html [cited Feb. 2003].

and this needs to be examined carefully. Among the terms that must be discussed, for example, is

$$\overline{f_x(\lambda T_x)_\eta}$$

(the overbar denotes an average), and the only way to determine whether this term is important is from Rocfire simulations. These simulations are also needed to provide a crucial boundary condition for the average of Eq. (8), one corresponding to the gradient condition (3).

The averaging is carried out in the context of a periodic propellant with x-wise period $2L$ (Ref. 5). Then the spatial average is defined by

$$\overline{(\cdot)} = \frac{1}{2L}\int_{-L}^{+L}(\cdot)\,\mathrm{d}x, \qquad \eta = \text{constant} \tag{9}$$

In addition, it is useful to eliminate small-timescale fluctuations by supplementing (9) with the time average

$$\frac{1}{\Delta t}\int_{t}^{t+\Delta t}(\cdot)\,\mathrm{d}t$$

where Δt is small on the timescale of any imposed pressure fluctuations, and small enough that the average does not affect the time derivatives in Eq. (8); a typical value is $\Delta t = 2\times 10^{-5}$s. Subsequently, when we refer to the spatial average (9) this time component is implicitly included.

Each variable (ρ, T, f, λ) is now written as the sum of its average and the deviation from that average, that is,

$$(\cdot) = \overline{(\cdot)} + (\cdot)' \tag{10}$$

Then Eq. (8) is average to yield

$$c\bar{\rho}(\overline{T_t} - \bar{f}_t\overline{T_\eta}) = (\bar{\lambda}\overline{T_\eta})_\eta + S \tag{11}$$

where

$$S = -c\overline{\rho' T_t'} + c\bar{f}_t\overline{\rho' T_\eta'} + c\bar{\rho}\overline{f_t' T_\eta'} + c\bar{T}_\eta\overline{\rho' f_t'}$$

$$+ c\overline{\rho' f_t' T_\eta'} + \overline{(\lambda' T_\eta')_\eta} + \overline{f_x'^2(\lambda T_\eta)_\eta} - \overline{f_x'(\lambda T_x)_\eta} = \sum_{n=1}^{8} S_i \tag{12}$$

In deriving this equation, we note the following: The term $(\lambda T_x)_x$ in Eq. (8) averages to zero because of the periodicity, and the terms $f_x(\lambda T_\eta)_x$, $f_{xx}\lambda T_\eta$ sum to $[f_x(\lambda T_\eta)]_x$, which likewise averages to zero.

That it would be unwise to simply assume that the terms in S can be neglected is shown by a simple example. Consider a block of propellant, periodic in x with width $2L$, and of thickness H. Both H and L are assumed to be much larger than any of the AP particles, all of which are modeled as circular discs. A uniform temperature T_2 is assigned at the surface $n=0$, a uniform temperature T_1 is assigned at the surface $n=-H$, and the goal is to calculate the total heat flux from one surface to the other, the governing equation being

$$(\lambda T_x)_x + (\lambda T_n)_n = 0 \tag{13}$$

Applying the averaging procedure to Eq. (13) yields

$$\left(\bar{\lambda}\bar{T}_n + \overline{\lambda' T_n'}\right)_n = 0 \tag{14}$$

whence the average heat flux (a constant) is

$$q = \bar{\lambda}\bar{T}_n + \overline{\lambda' T_n'} \tag{15}$$

Because L is large, $\bar{\lambda}$ will be constant, and integrating Eq. (15) over the depth yields

$$q = \frac{\bar{\lambda}(T_2 - T_1)}{H} + \frac{1}{H}\int_{-H}^{0}\mathrm{d}n\,\overline{\lambda' T_n'} \tag{16}$$

But because L is large, $\overline{\lambda' T_n'}$ will also be constant (except in small neighborhoods of the two surfaces, whose contribution to the integral is small), and so

$$q = \bar{\lambda}[(T_2 - T_1)/H] + \overline{\lambda' T_n'} \tag{17}$$

But we know, from the homogenization study of Ref. 6, where the properties of fine AP/binder blends are discussed, that

$$q = \lambda_{\text{homog.}}[(T_2 - T_1)/H] \tag{18}$$

where $\lambda_{\text{homog.}}$ is given by the formula

$$1 = (1-\alpha_v)^2[(1-x)/(\mathcal{F}-x)]^2\mathcal{F} \tag{19}$$

where $\mathcal{F} = \lambda_{\text{homog.}}/\lambda_{\text{binder}}$, $x = \lambda_{\text{AP}}/\lambda_{\text{binder}}$, and α_v is the volume fraction of AP. Thus,

$$\overline{\lambda' T_n'} = (\lambda_{\text{homog.}} - \bar{\lambda})[(T_2 - T_1)/H] \tag{20}$$

Note that because $\bar{\lambda}$ is the sum of the component values of λ each weighted by the fraction of the span $n=$ const. occupied by the component, and this sum is independent of n because the particles are much smaller than L, then

$$\bar{\lambda}/\lambda_{\text{binder}} = x\alpha_v + (1-\alpha_v) \tag{21}$$

This linear dependence on α_v is quite different from Eq. (19).

Let us now turn back to Eq. (11) and the boundary conditions. The temperature is specified deep within the solid, that is,

$$\bar{T} \to T_o \qquad \text{as} \qquad \eta \to -\infty \tag{22}$$

and at the surface,

$$\bar{T}_\eta = g \qquad \text{at} \qquad \eta = 0 \tag{23}$$

whence, noting that the derivative of T normal to the surface in the physical variables can be written as

$$T_n = \sqrt{1+f_x^2}\,T_\eta - f_x T_x\Big/\sqrt{1+f_x^2} \tag{24}$$

it follows that

$$g = \overline{f_x' T_x'\left(1+f_x'^2\right)^{-1}} + \overline{T_n\left(1+f_x'^2\right)^{-\frac{1}{2}}} \tag{25}$$

It is now clear what needs to be done. Each of the terms in S must be examined, using Rocfire, to determine its importance, and $\bar{f}_t$ and g must be represented in some way. The latter can be done by constructing a look-up table using Rocfire, and most of the computational burden comes from the construction of this table.

III. Rocfire Simulations and the Look-Up Table

Rocfire is a numerical tool for solving the unsteady multidimensional heterogeneous propellant combustion problem. The propellant is modeled by a distribution of AP disks (two-dimensional) or spheres (three-dimensional) embedded in the fuel binder. The size distribution of these particles can be chosen to match those of industrial packs.[7] For the present purposes we use a stoichiometric pack with four particle (disk) diameters: 106, 64.8, 52.3, and 44 μm. The corresponding volume fractions of AP are 0.6670, 0.0935, 0.0397, and 0.0199; the remaining 18% of total volume is binder. Each finite pack is a single element in a doubly infinite periodic assembly so that a pack of width $2L$ (x-wise) supports a combustion field with period $2L$. The pack thickness (y-wise) can be chosen independently.

Figure 1 shows four packs, of different widths, used to explore the effect of the width on the burning history. The thickness of each pack is approximately 500 μm, and the widths are $L = 93.6$ μm, 859.0 μm, 2356.8 μm, and 6076.9 μm. Negligibly small variations in the total volume fraction of AP (essentially 82%) are identified in the figure caption.

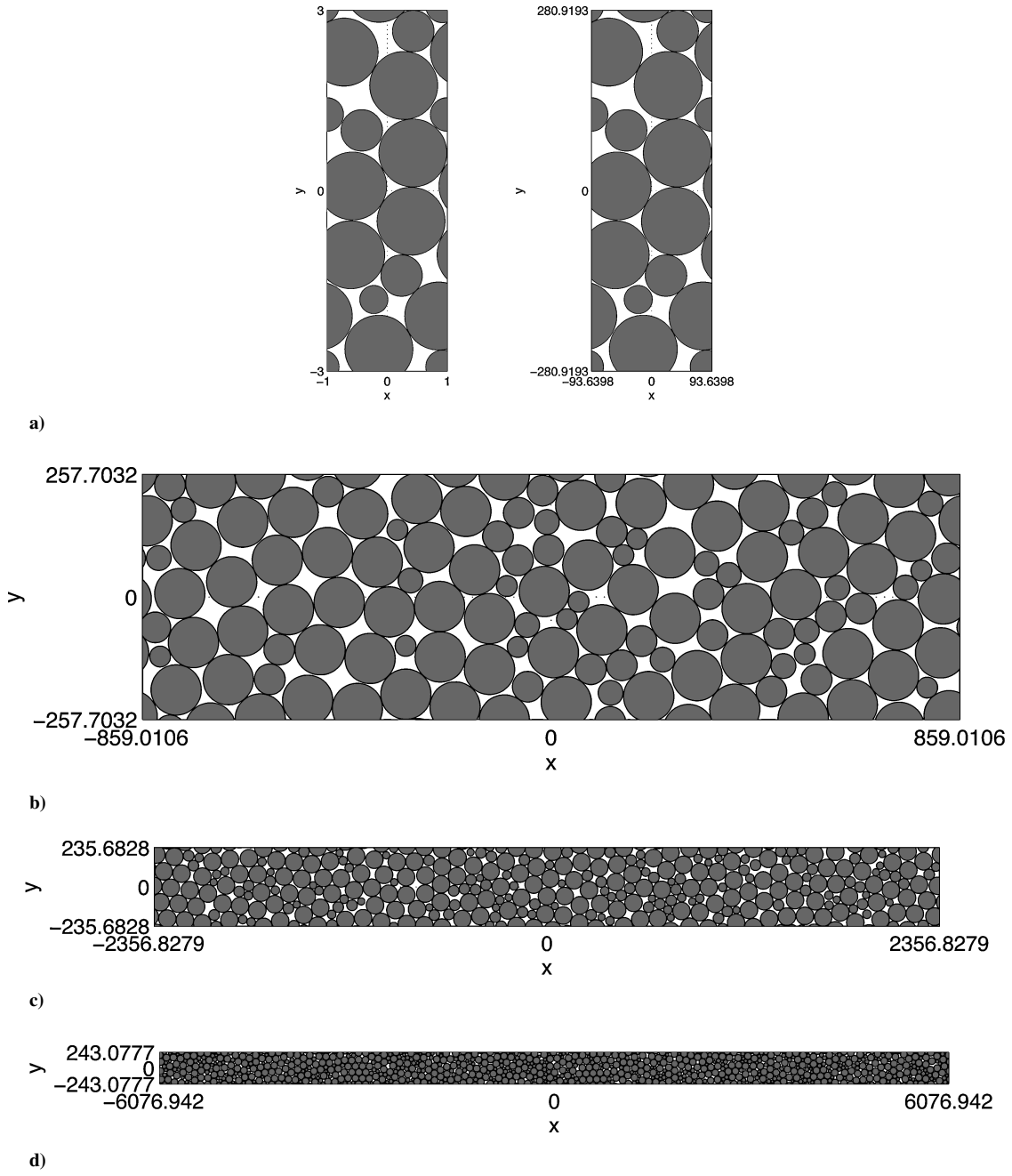

Fig. 1 Two-dimensional pack used for the calculations for varying domain length: a) $L = 93.64$ μm, $\alpha_v = 0.82052$; b) $L = 859.01$ μm, $\alpha_v = 0.82006$; c) $L = 2356.83$ μm, $\alpha_v = 0.82002$; and d) $L = 6076.94$ μm, $\alpha_v = 0.82000$. Here, α_v is the volume packing fraction. The disk diameters are 106, 64.8, 52.3, and 44.0 μm.

When these packs are burned, the results are as shown in Fig. 2. The propellant supply temperature T_o is 300 K, the pressure is 20 atm., the number of mesh points n_x is identified in the caption, and the model details and parameter values are those of Ref. 8. (Reference 9, a recent refinement, uses different parameters.) Each of the four panels in Fig. 2 shows time variations of the surface-averaged mass flux, the surface-averaged surface regression speed, and the surface-averaged normal temperature gradient at the surface. These are defined as follows:

$$\hat{M} = \frac{1}{2L}\int_{-L}^{+L} \mathrm{d}x\sqrt{1+f_x^2}M = -\overline{\rho f_t} \tag{26}$$

$$\hat{r}_b = \frac{1}{2L}\int_{-L}^{+L} \mathrm{d}x\sqrt{1+f_x^2}r_b = -\bar{f}_t \tag{27}$$

$$\hat{h} = \frac{1}{2L}\int_{-L}^{+L} \mathrm{d}x\sqrt{1+f_x^2}\,T_n = \overline{-f_x T_x + T_y} \tag{28}$$

Here, temperature gradients are evaluated on the solid side of the propellant surface, and the kinematic equation

$$f_t + r_b\sqrt{1+f_x^2} = 0 \tag{29}$$

relates the local regression speed to the derivatives of the surface function f (Ref. 2).

Following an initial transient, all variables settle down to a fluctuation about a mean, periodic in the pack burn-through time. (Pack burn-through is marked by the vertical lines in Fig. 2.) These fluctuations arise because the average nature of the surface changes with time, but these changes diminish in magnitude with increasing L. There is, accordingly, some merit in choosing a large value of L if the goal is to use these simulations to generate an x-averaged description. But the computational costs are high, particularly for the three-dimensional problem, and an alternative strategy is to use a modest value of L and use time averaging as a surrogate for the

Table 1 Space–time averages as a function of domain size L and grid size $\Delta x = 2L/n_x$

L	n_x	Δx, μm	$\hat{r}_b$	$\hat{M}$	$\hat{h}$
93.6398	80	2.34	0.70301744	1.22752448	242,874.1162908
93.6398	160	1.17	0.69900609	1.22923977	239,796.1264436
859.0106	320	5.37	0.69464096	1.23394854	242,426.9975635
859.0106	640	2.68	0.70271038	1.24963211	242,599.8956453
2356.8279	640	7.37	0.69382329	1.23876522	245,643.8986719
2356.8279	1280	3.68	0.70399859	1.24964381	246,402.1837242
6076.9420	6000	2.03	0.71833545	1.25647660	244,475.8223880

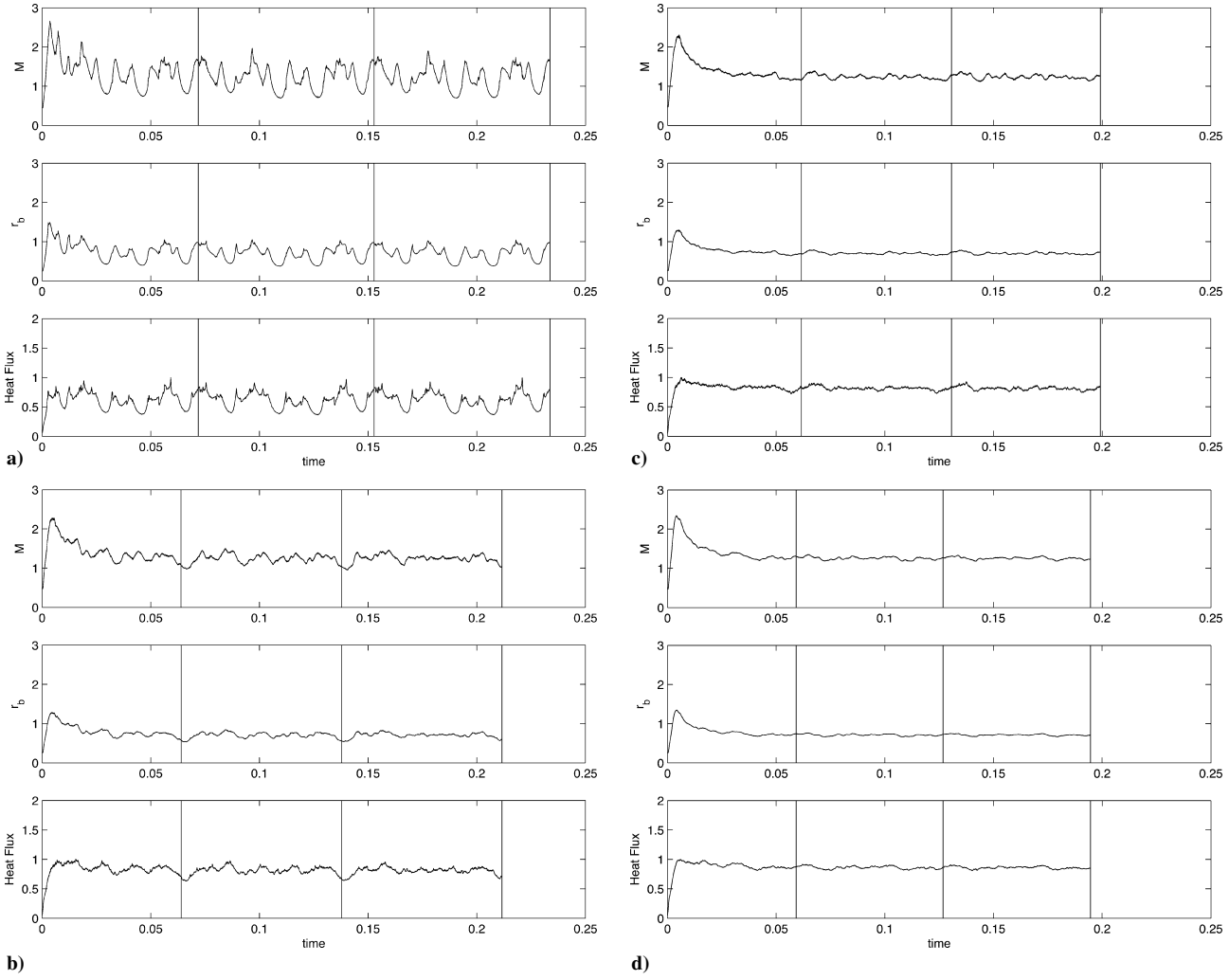

Fig. 2 Time-dependent averaged mass flux, speed, and heat flux at $P = 20$ atm and $T_o = 300$. Results for a) $L = 93.6$ μm, $n_x = 80$; b) $L = 859.0$ μm, $n_x = 640$; c) $L = 2356.8$ μm, $n_x = 640$; and d) $L = 6076.9$ μm, $n_x = 6000$.

greater spatial averaging. It is appropriate to take this temporal average over the burn-through period of a single pack.

Table 1 shows $\hat{r}_b$, $\hat{M}$, and $\hat{h}$ for the various L and different grid sizes. Clearly the smallest L (93.64 μm) and the coarsest mesh ($\Delta x = 2.34$ μm) are sufficient for our purposes.

A. Constructing the Look-Up Table

The strategy for constructing the look-up table is rooted in the following observation. If we specify the surface topography f and composition, the surface temperature T_s, the surface mass flux M, and the gas pressure P (spatially uniform in the low-Mach-number combustion field), then the combustion field is uniquely determined. (This is the key to the ZN strategy for discussing the one-dimensional unsteady burning of homogeneous propellants, with the heat flux from the combustion field to be determined experimentally.) Moreover, the desired averages, such as g, can be calculated.

The difficulty here is the specification of f and T_s [M is known if T_s is assigned when individual pyrolysis laws of the form (4) are assumed for each propellant component, as in Refs. 2 and 8]. One strategy for dealing with this is to use T_o as a single controlling parameter (with P fixed) for the specification of f and T_s. The values of T_o have nothing to do with the physical values to be used in the Rocburn module (except for the relatively uninteresting case of steady burning) but are virtual values used solely to construct the combustion field and therefore the heat flux at the surface and the other ingredients of Eq. (11). The look-up table is then constructed from two input parameters $T_{o\text{virtual}}(i)$, $i = 1, \ldots, N_1$, $P(j)$, $j = 1, \ldots, N_2$, and can contain whatever variables are of interest. For example, Eq. (11) contains $-\bar{f}_t$, defined by Eq. (9) but to be replaced by

$$\frac{1}{T} \cdot \frac{1}{2L} \int_0^T \mathrm{d}t \int_{-L}^{+L} \mathrm{d}x(-f_t) \tag{30}$$

as determined by the Rocfire calculation. A graphical representation of the tabular entry $-\bar{f}_t(i, j)$ is shown in Fig. 3, and the

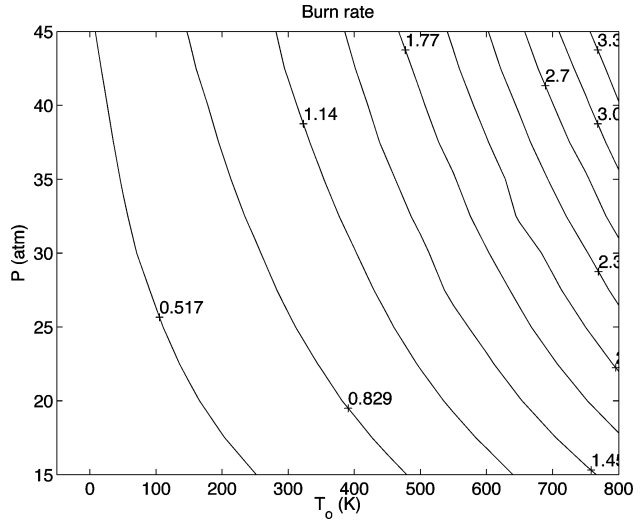

Fig. 3 Mean regression rate.

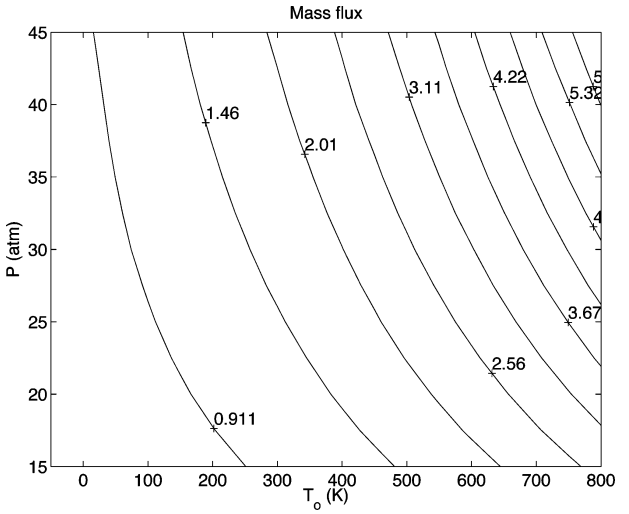

Fig. 4 Mean mass flux.

corresponding variations of the mass flux [compare Eq. (26)] are shown in Fig. 4. Figure 5 shows the mean temperature gradient [compare Eq. (28)].

Of particular relevance is the entry $g(i, j)$ needed for the boundary condition (23), but in addition, because we do not have an averaged pyrolysis law relating $\hat{M}$ and $\bar{T}_s$, $\bar{T}_s(i, j)$ must also be added to that table so that the relation between $\hat{M}$ and $\bar{T}_s$ is via the tabular entries. (The homogenization formula derived for a fine-AP/binder blend in Ref. 6 cannot reliably be used as it is derived assuming that the length scale of the heterogeneities is small compared to other relevant length scales, such as the flame stand-off distance.)

Rocfire uses the mapping (7) so that g can be obtained directly without explicit use of the relation (25).

B. Accuracy of Table Look-Up

There are various sources of error in the strategy just outlined. One is the use of T_o as a controlling parameter for generating the surface fluctuations that define $\bar{f}_t$ and $\bar{T}_s$. Another is the look-up algorithm itself. The latter can be independently investigated by examining a homogeneous propellant, a fine-AP/binder blend, which supports a one-dimensional combustion field. To this end we have numerically burned a blend with AP volume fraction 0.87 (this has the same steady burn rate as the pack when $P = 20$ atm) and subjected it to a pressure pulse

$$P_{\text{pulse}}(t) = P_0 + (P_1 - P_0)\exp\left[-(t - t_h)^2/\delta^2\right]$$
$$P_0 = 20 \text{ atm}, \qquad P_1 = 40 \text{ atm} \tag{31}$$

The term $(\mathrm{d}P/\mathrm{d}t)(t)$ is retained in the gas-phase energy equation.

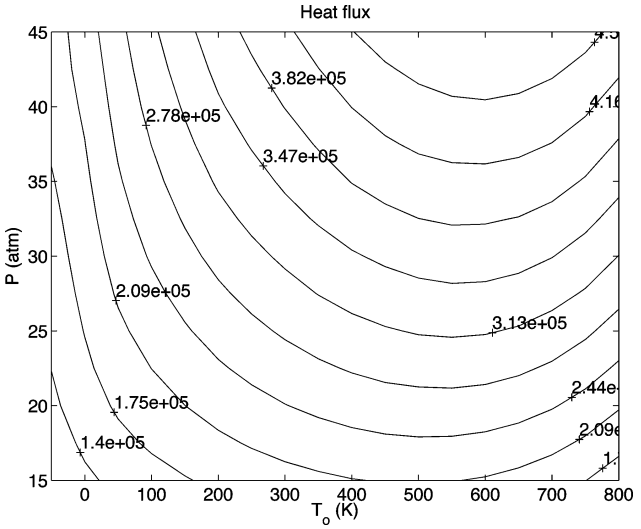

Fig. 5 Mean temperature gradient.

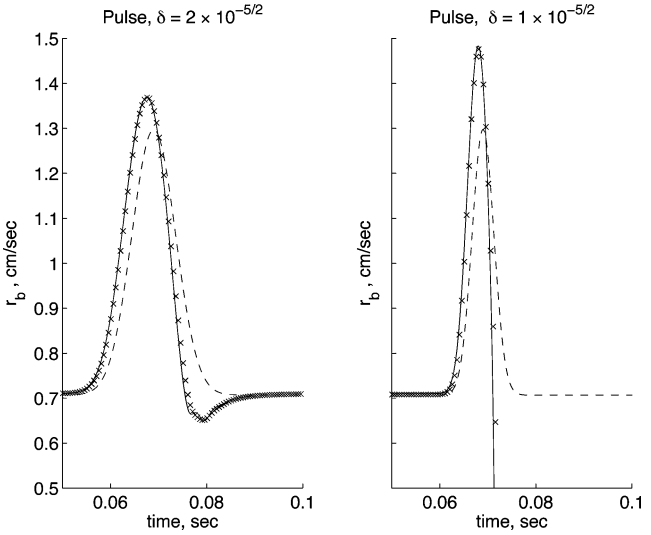

Fig. 6 One-dimensional blend burn-rate response to the pressure pulse: ——, numerical solution; ×, table solution; and – – –, steady burn-rate response.

Figure 6 shows the burn-rate history for $\delta = 2 \times 10^{-2.5}$ s and $1 \times 10^{-2.5}$ s. The solid line is the numerical solution (one-dimensional Rocfire), and the symbols are derived by solving the heat equation in the solid and using a look-up table. [The dashed line is the quasi-steady (solid- and gas-phase) solution.] The agreement is excellent. Moreover, the table approach can correctly predict quenching when δ is small enough. Quenching occurs because the sharp drop in pressure at the back of the pulse causes a sharp drop in flame speed, yet the mass flux off the surface has risen beyond the 20-atm value during the pulse, cannot drop so rapidly, and the flame is blown off.

Quenching does not occur for the pack when $\delta = 10^{-2.5}$ s (Fig. 7). Also, this figure shows that it is not necessary to retain $(\mathrm{d}P/\mathrm{d}t)(t)$ in such calculations.

IV. Discussion of the Averaged Terms Defining S

In this section we shall examine in detail the contribution that the source term S plays in the solution of the averaged temperature equation (11). First, however, we rewrite it using $\rho_{\text{homog.}}$ rather than $\bar{\rho}$ and $\lambda_{\text{homog.}}$ rather than $\bar{\lambda}$. Note that $\bar{\rho} = \rho_{\text{homog.}}$ in the limit $L \to \infty$, so that $\rho_{\text{homog.}}$ is a natural choice for the average density, but the claim for $\lambda_{\text{homog.}}$ as the average conductivity is weaker. It has the advantage that it is the correct choice for the fine-AP/binder blend

limit. Then

$$c\rho_{\text{homog.}}(\bar{T}_t - \bar{f}_t\bar{T}_\eta) = \lambda_{\text{homog.}}\bar{T}_{\eta\eta} + \sum_{n=1}^{10} S_n \tag{32}$$

where

$$S_9 = -c(\bar{\rho} - \rho_{\text{homog.}})(\bar{T}_t - \bar{f}_t\bar{T}_\eta) \tag{33}$$

$$S_{10} = [(\bar{\lambda} - \lambda_{\text{homog.}})\bar{T}_\eta]_\eta \tag{34}$$

Also, before continuing, it is useful to write out the components of S_7 and S_8:

$$S_7 = \overline{f_x'^2}(\overline{\lambda T}_\eta)_\eta + \overline{f_x'^2(\bar{\lambda}T_\eta')}_\eta + \overline{f_x'^2(\lambda'\bar{T}_\eta)}_\eta + \overline{f_x'^2(\lambda'T_\eta')}_\eta$$

$$= \sum_{m=1}^{4} S_{7,m} \tag{35}$$

$$S_8 = -\overline{f_x'(\bar{\lambda}T_x')}_\eta - \overline{f_x'(\lambda'T_x')}_\eta = \sum_{m=1}^{2} S_{8,m} \tag{36}$$

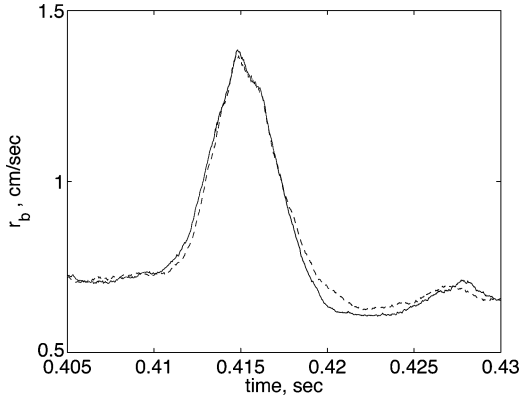

Fig. 7 Heterogeneous propellant burn-rate response to the pressure pulse: ——, inclusive of the pressure variation term and – – –, obtained by setting $dP_0/dt = 0$ in the gas phase.

To identify which of the various S_i are important, Rocfire calculations are carried out for two time-dependent pressures, the pulse defined by Eq. (31) with $\delta = 10^{-2.5}$ s, and a ramp defined by

$$P_{\text{ramp}} = \tfrac{1}{2}(P_0 + P_1) + \tfrac{1}{2}(P_1 - P_0)\tanh[(t - t_h)/\delta]$$

$$P_0 = 20 \text{ atm}, \qquad P_1 = 40 \text{ atm}, \qquad \delta = 10^{-3} \text{ s} \tag{37}$$

For this purpose, the narrow pack ($L = 93.6\ \mu$m) used to generate the look-up table for Rocburn is not appropriate, as the results are then dependent on the choice of t_h, and so the wider pack of half-width 6076.9 μm is used.

Figure 8 shows variations of the time averaged S_i, $i = 1, \ldots, 8$, for the pressure pulse. These averages are taken over the pulse width of $10^{-2.5}$ s. For reference purposes, the first panel shows variations of $\lambda_{\text{homog.}}\ \bar{T}_{\eta\eta}$ averaged over the burn-through period. We do not show S_9 and S_{10}, both of which behave roughly like $\bar{T}_{\eta\eta}$, but consider their magnitudes later.

The normalized spatial integrals of the S_i can be defined by

$$S_i^* = \frac{\int_{-\infty}^{0} S_i\ \mathrm{d}\eta|_{\text{average}}}{\int_{-\infty}^{0} \lambda_{\text{homog.}}\bar{T}_{\eta\eta}|_{\text{average}}} \tag{38}$$

and the values are shown in Table 2 for both the pressure pulse and the pressure ramp. The largest terms are S_2^*, S_3^*, S_6^*, and S_7^*, both for the pulse and the ramp, and we shall argue that only these are candidates for inclusion in Rocburn.

The key measure of the importance of each S_i is the contribution that it makes to the mean surface temperature, as this controls the burning rate. Each contribution can be evaluated in the following fashion.

Equation (32) is a linear inhomogeneous equation for $\bar{T}$, which can be solved, and the mean surface temperature evaluated, if $\bar{f}_t$ and the S_i are assigned: $\bar{f}_t$ is assigned from Rocfire, but each S_i is either assigned from Rocfire, or set to zero. Thus the dashed curves in each panel of Fig. 9 show the time variations of surface temperature during the pressure pulse when all of the S_i are set equal to zero. The solid curves, on the other hand, are derived directly from Rocfire, so that the difference between the solid and dashed curves is a measure of the total contribution of all the S_i. The average difference is roughly 25 K. To confirm the accuracy of the calculations, the total

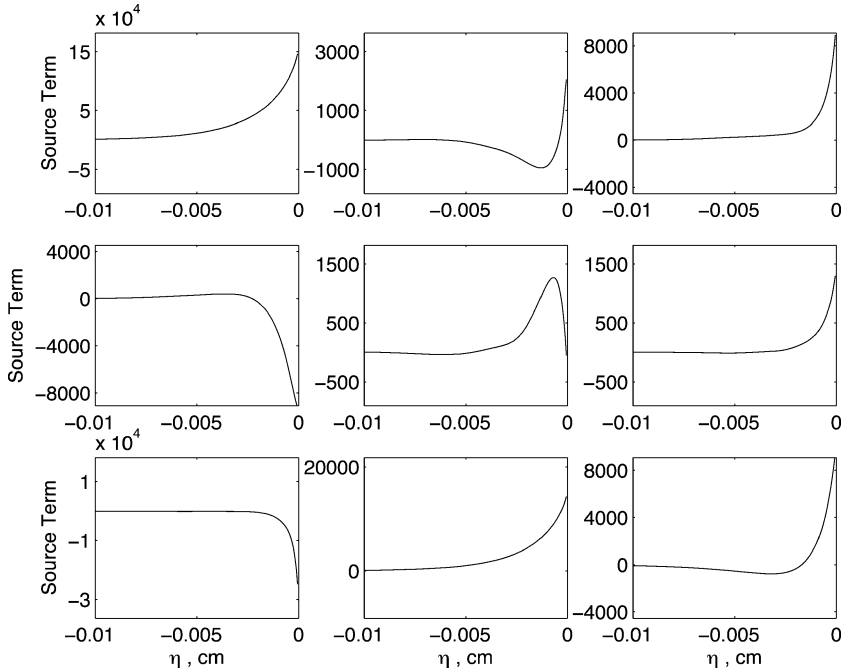

Fig. 8 Response to the pressure pulse: source-term spatial variations. The first panel shows $\lambda_{\text{homog.}}\ \bar{T}_{\eta\eta}$; the remainder show S_i, $i = 1, 8$ (left to right, top to bottom).

Table 2 Integrated source-term contributions

Pressure	S_1^*	S_2^*	S_3^*	S_4^*	$S_{5,*}$	$S_{6,*}$	$S_{7,*}$	$S_{8,*}$
Rise	-6.9×10^{-3}	$+2.5\times10^{-2}$	-2.2×10^{-2}	$+7.2\times10^{-3}$	$+2.9\times10^{-3}$	-3.9×10^{-2}	$+6.9\times10^{-2}$	$+6.3\times10^{-3}$
Pulse	-6.9×10^{-3}	$+2.4\times10^{-2}$	-2.0×10^{-2}	$+6.7\times10^{-3}$	$+2.7\times10^{-3}$	-4.2×10^{-2}	$+8.4\times10^{-2}$	$+7.0\times10^{-3}$

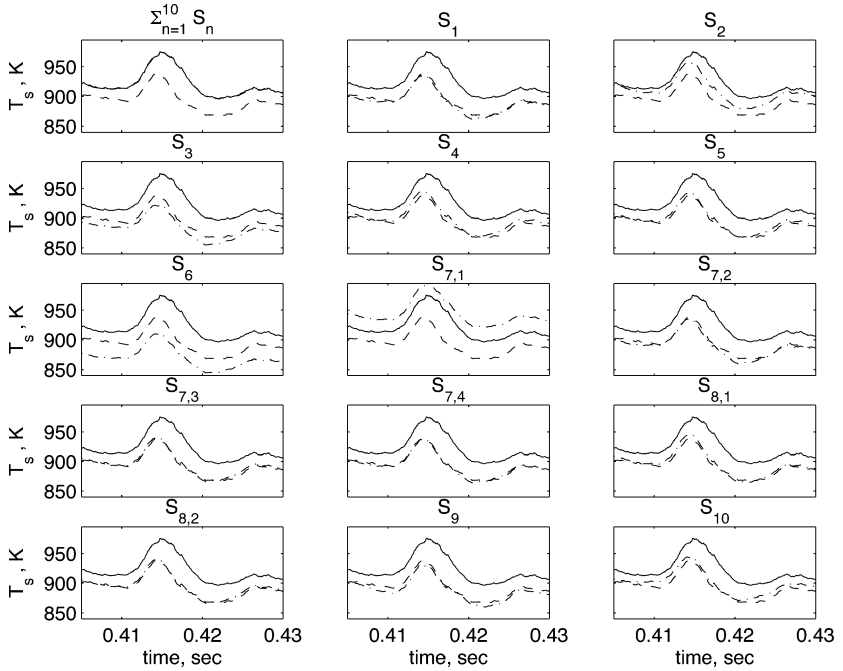

Fig. 9 Response to the pressure pulse: source-term contributions to the surface temperature.

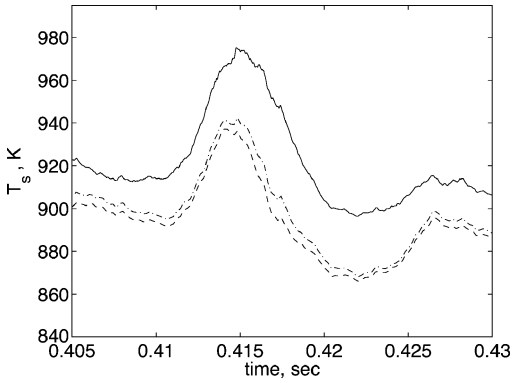

Fig. 10 Contribution of the convective terms $S_2+S_3+S_4+S_5$ to the surface temperature.

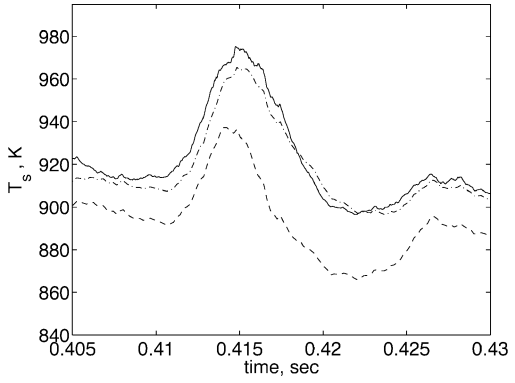

Fig. 11 Contributions of $S_{\text{effective}}$ to the surface temperature.

contribution is also evaluated by integration of Eq. (32) and plotted in the first panel of Fig. 9; it cannot be distinguished from the Rocfire calculation.

Each remaining panel in Fig. 9 shows the contribution from a single S_i (the dash–dot curves). A significant role is played by S_2, S_3, S_6, and $S_{7,1}$, with S_{10} a runner up whose contribution, as for all smaller ones, we shall ignore. Moreover, when the convection terms (proportional to c) S_2, S_3, S_4, and S_5 are added together, they cancel to a large extent (Fig. 10). And so if only S_6 and $S_{7,1}$ are retained to define an approximation to S, namely,

$$S_{\text{effective}} = S_6 + S_{7,1} = \overline{(\lambda' T_\eta')_\eta} + \overline{f_x'^2}(\bar{\lambda}\bar{T}_\eta)_\eta \tag{39}$$

decent agreement with the exact solution is achieved (Fig. 11).

How general this conclusion might be is hard to say, although a number of numerical experiments for different pressure histories show comparable agreement. And of course, all of the results are within the context of the particular Rocfire model that we have used, and adjustments to the model (to the kinetics for example) could change things. But the strategy laid out here is a universal one.

V. Modeling the Source Term $S_{\text{effective}}$

To complete the specification of the Rocburn module, it is necessary to model the two terms that contribute to $S_{\text{effective}}$. The first of these S_6 arises directly from the heterogeneity of the propellant, and the second $S_{7,1}$ from surface corrugations. S_6 is negative, with a surface value -27468.7 cal/cm^{3}s, and $S_{7,1}$ is positive with a surface value 14265.4 cal/cm^{3}s (Fig. 8).

Because S_6 originates in the term $(\lambda T_\eta)_\eta$, we adopt the rough model for it defined by

$$S_{6,\text{model}} = \chi \lambda_{\text{homog.}} \bar{T}_{\eta\eta}, \qquad \chi = -3.0\times10^{-2} \tag{40}$$

which is compared with the exact function (both averaged over a period) in Fig. 12. The depth or skin thickness of the approximation is greater than that of the exact function, and this is compensated by a smaller surface value. Clearly there is room here for better approximations, but the important thing is to capture the surface temperature correctly, and, as will be apparent shortly, Eq. (40) suffices for this purpose.

To model $S_{7,1}$, it is necessary to model $\overline{f_x'^2}$. This can be constructed as part of the look-up table from Rocfire, but variations with the mean

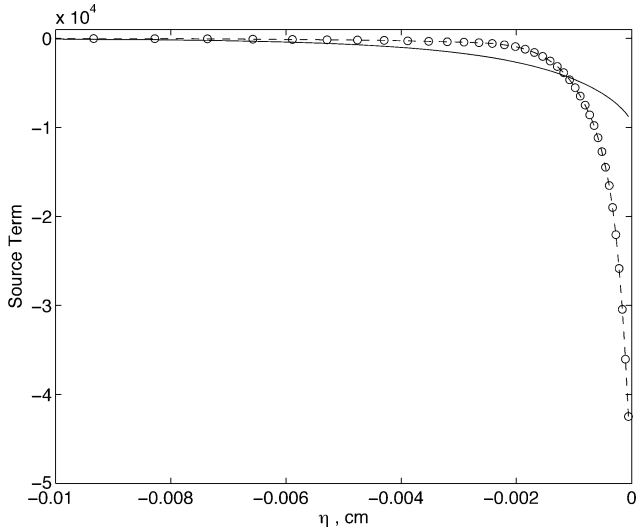

Fig. 12 Period average of S_6 (○) compared with $S_{6,\text{model}}$ (——).

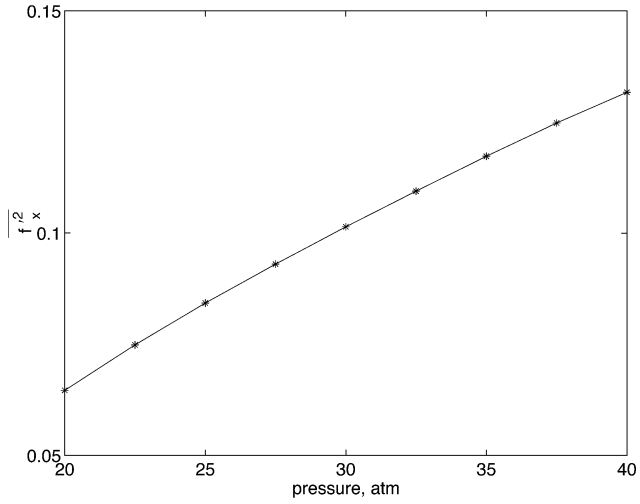

Fig. 13 Corrugation of the surface as a function of pressure.

surface temperature, pressure fixed, are modest, and so we shall be content with assuming that it depends only on pressure, and then Fig. 13 can be constructed. Comparisons between the approximation and the exact function are shown in Fig. 14 for both the pressure rise and the pressure pulse, and there are errors in the final relaxation to steady state.

Despite the imperfections in the modeling of S_6 and $S_{7,1}$, we combine them in the form

$$S_{\text{effective, model}} = \left[\chi + \overline{f_x'^2}(P)\right]\lambda_{\text{homog.}}\bar{T}_{\eta\eta} \tag{41}$$

and this provides a decent approximation to the surface temperature (Fig. 15).

VI. Model That Eliminates S

Consider the terms on the right-hand side of Eq. (32) that depend on λ. They are

$$\lambda_{\text{homog.}}\bar{T}_{\eta\eta} + \overline{(\lambda' T_\eta')_\eta} + \overline{f_x'^2(\lambda T_\eta)_\eta} - \overline{f_x'(\lambda T_x)_\eta} + [(\bar{\lambda} - \lambda_{\text{homog.}})\bar{T}_\eta]_\eta \tag{42}$$

and when integrated over the thermal layer

$$\left[\int_{-\infty}^{0} (\cdot)\,\mathrm{d}\eta\right]$$

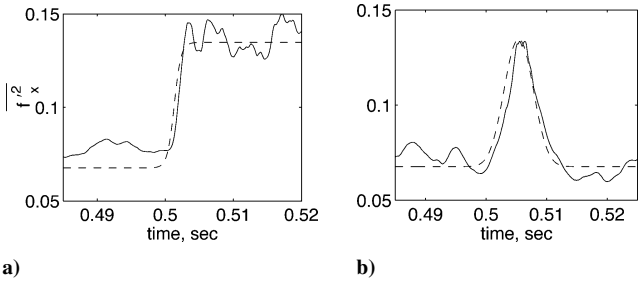

Fig. 14 Time variation of $\overline{f_x'^2}$ with the a) pressure rise and b) pressure pulse: ——, exact values and – – –, model values.

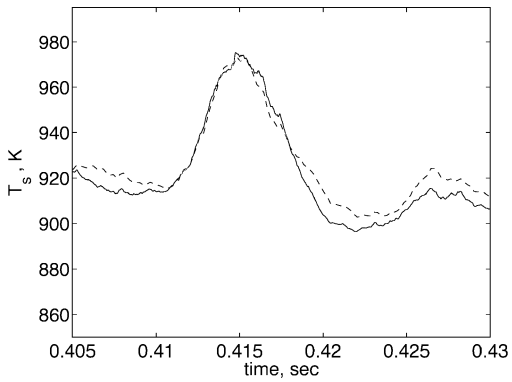

Fig. 15 Surface-temperature variations: ——, Rocfire and – – –, $S_{\text{effective,model}}$.

become

$$\left[\bar{\lambda}\bar{T}_\eta + \overline{\lambda' T_\eta'} + \overline{f_x'^2\lambda T_\eta} - \overline{f_x'\lambda T_x}\right]_{\eta=0} \tag{43}$$

Now the heat flux at the surface (in the solid) through an element of surface of length $\sqrt{(1+f_x^2)}\,\mathrm{d}x$ is

$$Q\,\mathrm{d}x \equiv \lambda\frac{\partial T}{\partial n}\sqrt{1+f_x^2}\,\mathrm{d}x \tag{44}$$

so that, noting Eq. (24),

$$\bar{Q} = \left[\bar{\lambda}\bar{T}_\eta + \overline{\lambda' T_\eta'} + \overline{f_x'^2\lambda T_\eta} - \overline{f_x'\lambda T_x}\right]_{\eta=0} \tag{45}$$

which is identical to Eq. (43), an elementary consequence of energy conservation. And so a possible modeling strategy is to delete all terms in S (we have already observed that the convection terms can be neglected) and solve the equation

$$c\rho_{\text{homog.}}(\bar{T}_t - \bar{f}_t\bar{T}_\eta) = \lambda_{\text{homog.}}\bar{T}_{\eta\eta} \tag{46}$$

replacing the boundary condition (23) with

$$\lambda_{\text{homog.}}\bar{T}_\eta|_{\eta=0} = \bar{Q} = \frac{1}{2L}\int_{-L}^{+L}\mathrm{d}x\lambda\frac{\partial T}{\partial n}\sqrt{1+f_x^2} \tag{47}$$

where $\bar{Q}$ is defined by the look-up table. This modified boundary condition properly accounts for the global energetic consequences of S.

VII. Alternative Strategy for Constructing the Look-Up Table

It was noted earlier that the use of T_o as a controlling parameter for generating the look-up table is a potential source of error, and so here we describe an alternative, albeit more complicated, strategy. The essential idea is to run Rocfire for an extended period of time during which the pressure is varied and to make a large number of discrete observations of the look-up table components. For example, each observation will include a value of g, T_s, and P. It is quite possible, in principle, that two separate observations will have the same values

of $\bar{T}_s$ and P but different values of g, generated by different surface configurations. If such differences are always small, then the earlier strategy for determining $g(\bar{T}_s, P)$ suffices, but if that is not the case the earlier strategy will lead to error in certain circumstances. Then the goal is to construct a set of tabular values that represent the larger set of observations in some optimal fashion.

The procedure can be understood by examining the simplest case where the table contains a single dependent field $G_{ij}, i = 1, \ldots, M, j = 1, \ldots, N$ defined by the two independent fields $P_i, i = 1, \ldots, M, T_j, j = 1, \ldots, N$, both assigned. Here the $\{G_{i,j}\}$ are the values of g, the $\{P_i\}$ are the values of pressure, and the $\{T_j\}$ are the values of the mean surface temperature.

Consider now the set of observations (of pressure, mean surface temperature, and g)

$$E = \{(p_k, t_k, g_k) \quad k = 1, \ldots, L\} \tag{48}$$

obtained by sampling the Rocfire calculation at equal time intervals where $L \gg MN$, the number of independent entries in the table.

For each k, i^*, and j^* are defined by

$$P_{i^*} < p_k < P_{i^*+1}, \qquad T_{j^*} < t_k < T_{j^*+1}$$

and g_k is approximated by the bilinear interpolation formula

$$g_k \approx A_{1,1}G_{i^*,j^*} + A_{1,2}G_{i^*,j^*+1} + A_{2,1}G_{i^*+1,j^*} + A_{2,2}G_{i^*+1,j^*+1} \tag{49}$$

where

$$A = \frac{1}{(T_{j^*+1} - T_{j^*})(P_{i^*+1} - P_{i^*})} \times \begin{bmatrix} (T_{j^*+1} - t_k)(P_{i^*+1} - p_k) & (t_k - T_{j^*})(P_{i^*+1} - p_k) \\ (T_{j^*+1} - t_k)(p_k - P_{i^*}) & (t_k - T_{j^*})(p_k - P_{i^*}) \end{bmatrix}$$

In general i^* and j^* take the same values for more than one value of k.

The L equations defined by Eq. (49) can be written in matrix form

$$Dx = b \tag{50}$$

where b is the column vector of dimension L defined by the known $\{g_k\}$ and x is an appropriate column vector of dimension MN containing all of the $\{G_{i,j}\}$. Because the system (50) is overdetermined, any choice of x will generate a nonvanishing vector $b - Dx$. However, a least-squares approximation can be constructed by minimizing $(b - Dx)^T(b - Dx)$, the norm square of the residual. This solution is

$$x = [D^T D]^{-1} D^T b \tag{51}$$

and contains the entries $\{G_{i,j}\}$.

We have constructed a table in this fashion (the new table) using the pressure history of Fig. 16, sampled 10,026 times; the pulse ($\delta = 10^{-5/2}$s) and the ramp ($\delta = 10^{-3}$s) are part of this history. Only a restricted range of input values are considered, sufficient to analyze the test cases under investigation, and values of g calculated in this way are compared with the old table values in Fig. 17. There are noticeable differences, particularly for higher pressures and higher values of $\bar{T}_s$.

VIII. Test Calculations

In the earlier sections we have described two strategies for dealing with the source term S in the averaged heat equation in the solid, one in which it is replaced by the approximation $S_{\text{effective,model}}$ [Eq. (41)] and one in which it is discarded, but the surface boundary condition (25) is replaced by Eq. (47). In addition we have described two strategies for constructing the look-up table, one in which the supply temperature T_o is used as an input parameter to define the properties of the propellant surface and one in which a least-squares approximation is constructed from a large number of samplings during a burn with a time-dependent pressure. In this section we examine the

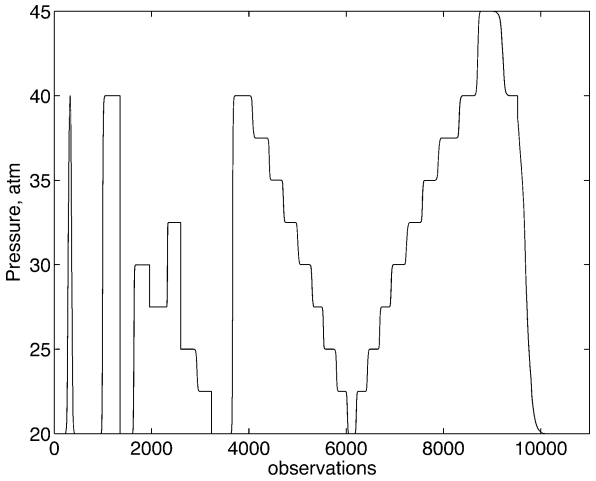

Fig. 16 Pressure history during the recording of the observation set.

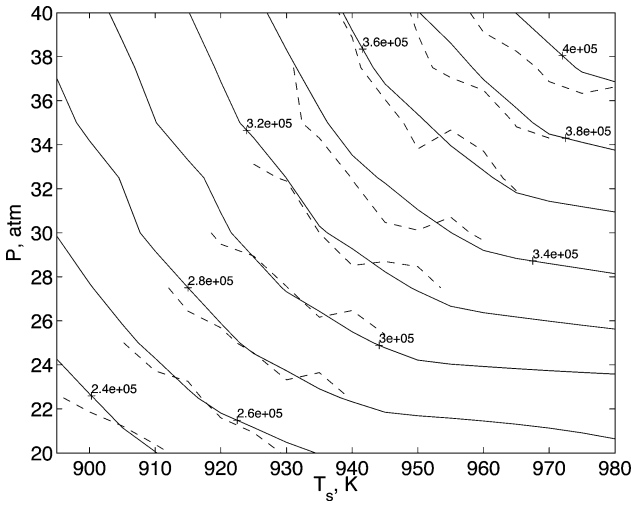

Fig. 17 Contour plot of the ——, old and – – –, new data sets for the function g.

accuracy of these strategies in the prediction of steady-state burning and the unsteady response to a pressure ramp and a pressure pulse. Three types of calculations are carried out: case 1, $S = 0$ with the modified boundary condition (47), the T_o-controlled table; case 2, S modeled by $S_{\text{effective,model}}$, the T_o-controlled table; and case 3, S modeled by $S_{\text{effective,model}}$, the table defined by sampling.

The results are shown in Figs. 18–20 with case 1 results in the top panels, case 2 results in the middle panels, and case 3 results in the bottom panels.

Figure 18 shows steady-state burning results for the mean surface speed and the mean surface temperature. The symbols are defined by Rocfire, and the solid curves by Rocburn. The third column of panels shows the errors, squares for the speed, and crosses for the temperature.

Case 1 yields the most accurate results, which is to be expected as the surface conditions that control the burning rate are defined by a global energy balance within the solid, which is exactly satisfied. Moreover, T_o as used in Rocburn and $T_{o\text{virtual}}$ as used to construct the look-up table are identical in the steady state, and so the table is constructed in optimal fashion. The errors in case 2 are only slightly higher than those of case 1, and differences reflect small errors in the global energy balance associated with the approximation to S. As for case 3, the table construction is not optimal, and the largest errors are generated, albeit quite acceptable. These errors would be smaller if the pressure history (Fig. 16) had longer time intervals in which the pressure field was held contant at the Rocfire values used in Fig. 18.

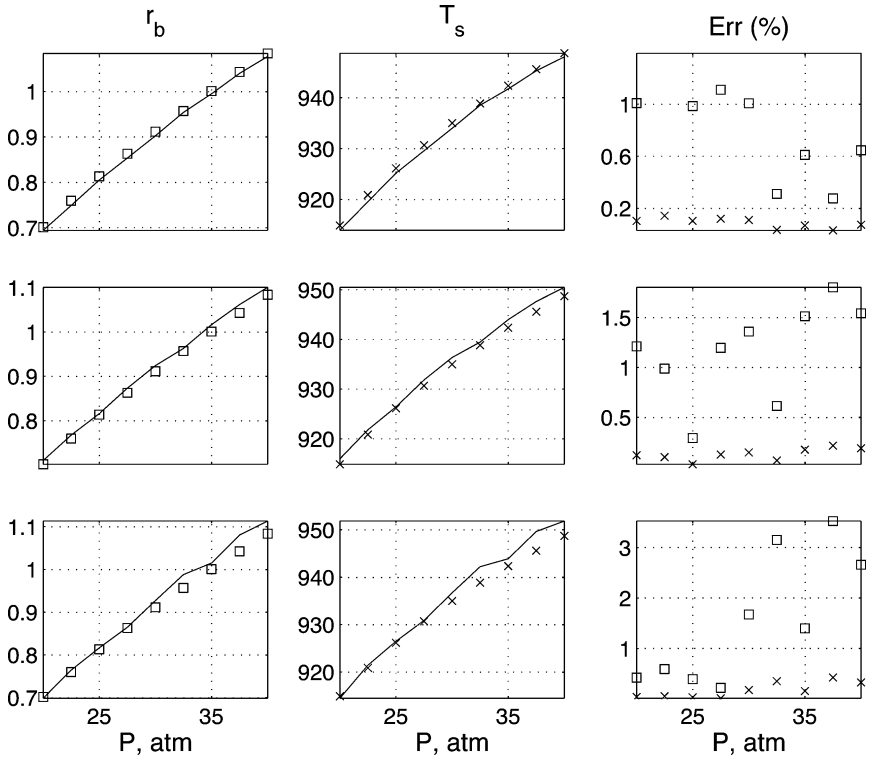

Fig. 18 Mean burning rate and surface temperature results for cases 1–3 compared with Rocfire.

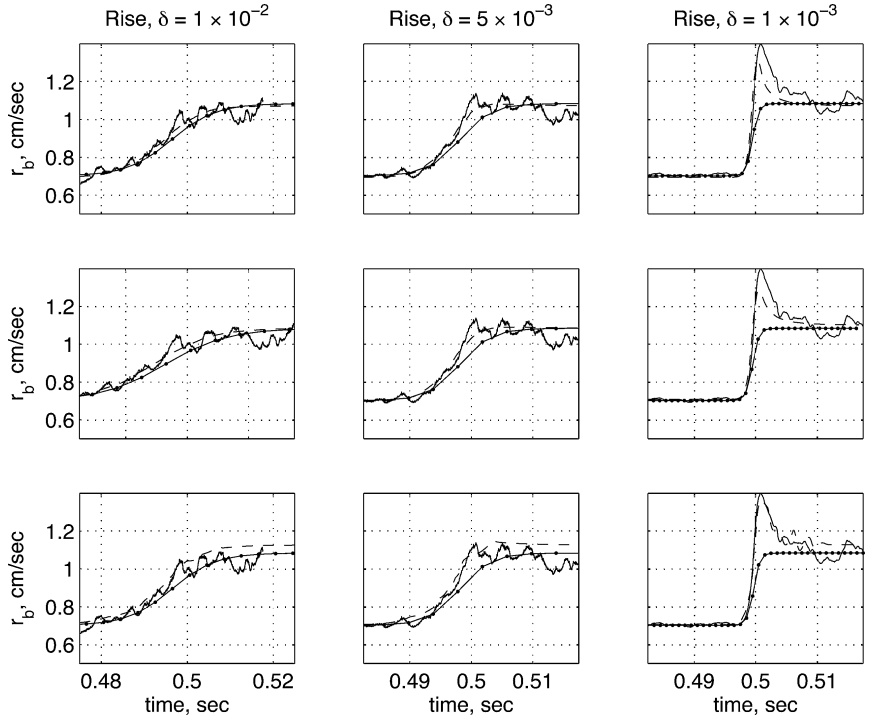

Fig. 19 Burning-rate histories for pressure ramps.

Figure 19 shows the response to three pressure ramps, of increasing severity. The wiggly solid curves are Rocfire result and would be smoother if larger values of the propellant width L were used. The smooth solid lines with dots are quasi-steady results in which transient storage of energy within the solid is not accounted for. The dashed curves are the Rocburn results.

The errors that arise when case 3 is used to calculate the steady burning rates, just noted, are apparent here as the pressure levels off and the burning rate approaches the steady value. But case 3 shines in capturing the overshoot for $\delta = 10^{-3}$s. Clearly the differences between the look-up tables shown in Fig. 17 play an important role during these high-pressure rapid transients.

Turning to the pressure-pulse responses (Fig. 20) here also it is the most rapid transients ($\delta = 10^{-5/2}$s) that provide the most severe test. Cases 1 and 2, unlike 3, fail to accurately predict the pressure peak. Case 1 exaggerates the undershoot. Case 3 recovers from the undershoot a little too quickly but is superior to case 2 in this respect.

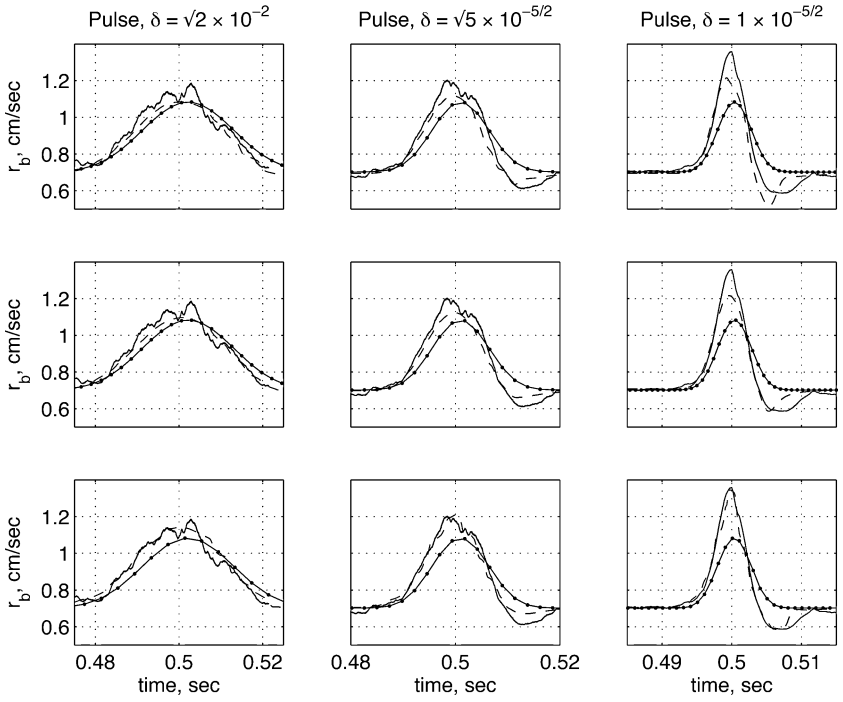

Fig. 20 Burning-rate histories for pressure pulses.

IX. Conclusions

In this paper we have described strategies that can be used to incorporate subgrid combustion ingredients into solid-propellant rocket simulations. Many of the specific details are not universal, for they depend on the direct-numerical-simulation calculations of the subgrid field, and so depend on a large number of model ingredients, imperfect at the present time, but the various strategies are universal and define a framework within which the details can be recalculated should the model be modified. To the best of our knowledge, the construction of such a framework has not previously been addressed.

To put these results in context, we note that they are the final set in a sequence of four, which, arguably, are the minimum required to define a combustion module (which we have called Rocburn) which can be coupled with chamber flow calculations for solid-propellant rockets. The other three are a packing code,[5,7] necessary to construct a reasonable model of the morphology of a heterogeneous propellant; an unsteady multidimensional code (which we have called Rocfire) capable of describing the combustion field supported by a heterogeneous propellant, coupled to heat-conduction processes within the propellant across the irregularly moving surface[2,8]; and homogenization tools, necessary to account for the contribution of AP particles so small as to be subgrid on the Rocfire scales.[6]

All of these tools are candidates for refinement, and any observation that some of our results are at variance with experiment merely informs the informed that refinement is necessary.[8] A recent refinement of Rocfire, incorporating an improved kinetics model, is described in Ref. 9. Furthermore, there are physical ingredients that could be added, but whose addition could hardly be called refinements. An example discussed in Ref. 4 is multivaluedness of the surface function f, an ingredient of propellants with cracks, and propellants with aluminum particles. Melt layers, near-surface heterogeneous reactions, the effects of erosive flowfields: these, and other ingredients, remain unaddressed.

Acknowledgments

This work was supported by the U.S. Department of Energy through the University of California under Subcontract B341494. Buckmaster is also supported by the Air Force Office of Scientific Research and by the NASA John H. Glenn Research Center at Lewis Field.

References

[1]Parsons, I. D., Alavilli, P., Namazifard, A., Acharya, A., Jiao, X., and Fiedler, R., "Coupled Simulations of Solid Rocket Motors," AIAA Paper 2000-3456, July 2000.

[2]Jackson, T. L., Buckmaster, J., "Heterogeneous Propellant Combustion," *AIAA Journal*, Vol. 40, 2002, pp. 1122–1130.

[3]Fiedler, R., Jiao, X., Namazifard, A., Haselbacher, A., Najjar, F., and Parsons, I. D., "Coupled Fluid-Structure 3-D Solid Rocket Motor Simulations," AIAA Paper 2001-3954, July 2001.

[4]Wang, X., Jackson, T. L., and Massa, L., "Numerical Simulation of Heterogeneous Propellant Combustion by a Level Set Method," *Combustion Theory and Modelling*, Vol. 8, 2004, pp. 227–254.

[5]Knott, G. M., Jackson, T. L., and Buckmaster, J., "The Random Packing of Heterogeneous Propellants," *AIAA Journal*, Vol. 39, 2001, pp. 678–686.

[6]Chen, M., Buckmaster, J., Jackson, T. L., and Massa, L., "Homogenization Issues and the Combustion of Heterogeneous Solid Propellants," *Proceedings of the Combustion Institute*, Vol. 29, 2002, pp. 2923–2929.

[7]Kochevets, S., Buckmaster, J., Jackson, T. L., and Hegab, A., "Random Packs and Their Use in the Modeling of Hetergeneous Solid Propellant Combustion," *Journal of Propulsion and Power*, Vol. 17, 2001, pp. 883–891.

[8]Massa, L., Jackson, T. L., Buckmaster, J., and Campbell, M., "Three-Dimensional Heterogeneous Propellant Combustion," *Proceedings of the Combustion Institute*, Vol. 29, 2002, pp. 2975–2983.

[9]Massa, L., Jackson, T. L., and Buckmaster, J., "New Kinetics for a Model of Heterogeneous Propellant Combustion," *Journal of Propulsion and Power* (to be published).

S. Mahalingam
Associate Editor